Impact of Photovoltaic System Integration on Total Harmonic Distortion in IEEE 9-Bus System

Amany Ali Abo-El-Hassan[1], Gaber El-Saady A. Taha[2], Ali M. Yousef[2] and El-Noby A. Ibrahim[2]
[1]Egyptian-German College of technology, Misr International Technological University, Assiut, Egypt
[2]Electrical Engineering Department., Faculty of Engineering, Assiut University, Assiut, Egypt.

Abstract

This research paper investigates the influence of photovoltaic (PV) array location on power quality within the context of an IEEE 9-bus system. As the global energy landscape shifts towards distributed generation (DG) renewable energy systems, understanding the dynamic interactions between PV systems and power grids becomes increasingly crucial. The study addresses a notable gap by comprehensively examining the impact of PV array location on total harmonic distortion (THD) under varying penetration levels. Leveraging mathematical modeling techniques and utilizing the IEEE 9-bus system as a benchmark, the research conducts a series of case studies involving load variations and sequential connections of PV systems to different buses. The findings underscore the importance of strategic PV array placement in mitigating harmonic distortion and ensuring power quality in grid-connected systems. Overall, this study contributes insights to the evolving field of renewable energy integration, emphasizing the significance of thoughtful PV system placement for enhancing grid stability and performance.

Keywords

Stability Analysis; PV system, PV penetration levels, IEEE Standard 9-Bus System, Total Harmonic Distortion (THD).

1. Introduction

Grid-connected PV systems, characterized by their ability to convert solar energy into electrical power and integrate it into existing utility grids, have witnessed remarkable growth and adoption worldwide. These systems, categorized as DG units, play a crucial role in meeting renewable energy targets, reducing carbon emissions, and enhancing grid resilience. With the increasing penetration of grid-connected PV systems, understanding their dynamic behavior, optimizing their performance, and mitigating associated challenges become imperative.

Numerous studies have explored the modeling, analysis, and optimization of grid-connected PV systems to address various technical and operational aspects. Previous research has focused on mathematical modeling of PV modules, power conditioning units, and grid integration strategies to enhance system efficiency and stability [1, 2]. Additionally, investigations into maximum power point tracking (MPPT) algorithms, control strategies for power converters, and voltage regulation techniques have been conducted to improve energy yield and grid compatibility [3, 4].

One notable area of concern in grid-connected PV systems is harmonic distortion, which can adversely affect power quality and grid stability. Harmonics, generated primarily by power electronic converters within PV inverters, introduce deviations from the sinusoidal waveform of voltage and current, leading to increased losses, equipment overheating, and electromagnetic interference [5, 6]. Previous studies have emphasized the importance of analyzing harmonic distortion and devising mitigation strategies to ensure compliance with grid codes and standards [7, 8].

In this context, this paper presents a comprehensive study on grid-connected PV systems, focusing on modeling, simulation, and analysis of system dynamics and harmonic distortion. The obtained results shed light on the impact of PV system placement on harmonic distortion levels within an IEEE 9-bus distribution network under various

*Corresponding author E-mail: eng.amanyali4@gmail.com
Received March, 31, 2024 received in revised form, April 9, 2024, accepted April 13, 2024.
(ASWJST 2021/ printed ISSN: 2735-3087 and on-line ISSN: 2735-3095) https://journals.aswu.edu.eg/stjournal

operational scenarios. Through detailed case studies, the paper evaluates the influence of PV system size, location, and penetration level on harmonic distortion, aiming to identify optimal deployment strategies for mitigating distortion effects and enhancing power quality in grid-connected environments. By building upon previous research and employing advanced modeling techniques, this study contributes to the ongoing efforts to optimize the integration of renewable energy sources and promote the reliable operation of modern power systems.

2. Modeling PV system

2.1 Mathematical equations

Grid-connected PV systems with high penetration, recognized as a type of DG in the megawatt range, are undergoing rapid development. These systems dominate the PV market in various countries worldwide. The primary elements of a grid-connected PV system comprise a combination of series/parallel-connected PV arrays for direct conversion of sunlight into DC power and a power-conditioning unit responsible for converting DC power to AC power while maintaining peak efficiency of the PVs. Figure. 1 illustrates the general diagram of grid-connected PV systems. It is noteworthy that, in numerous instances, energy storage devices, such as batteries and supercapacitors, are also considered as the third component of grid-connected PV systems. These devices enhance the overall performance of PV systems, facilitating functions like power generation during nighttime, reactive power control, peak load shifting, and grid voltage stabilization [9].

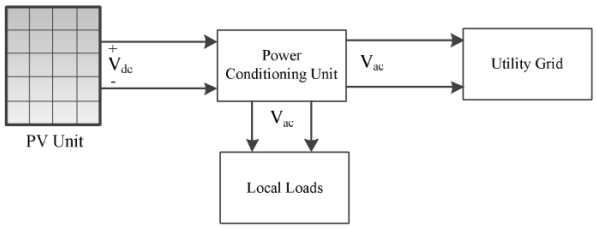

Figure 1. Basic illustration of a photovoltaic system connected to the grid.

Typically, the electrical characteristics of a PV unit are described in terms of the current-voltage or power-voltage relationships of the cell. These characteristics vary depending on the amount of solar irradiation received and the temperature of the cell. Thus, to analyze the dynamic performance of PV systems under different weather conditions, an accurate model is necessary to account for how changes in irradiance and temperature affect the current and voltage produced by the PV arrays.

Figure. 2 depicts the equivalent electrical circuit of a typical PV module, where I represents the output terminal current, I_L denotes the light-generated current, I_d signifies the diode current, I_{sh} indicates the shunt leakage current, R_s represents the internal resistance, and R_{sh} denotes the shunt resistance.

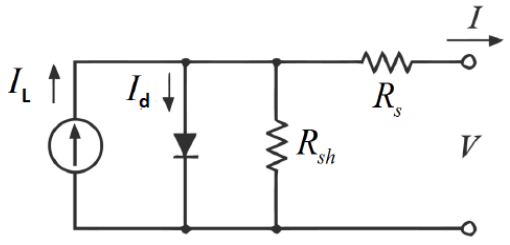

Figure 2. Circuit model that represents a PV module.

From Fig. 2, the output current (I) of the PV module can be expressed as:

$$I = I_L - I_d - \frac{V_o}{R_{sh}} \quad (1)$$

where V_o is the voltage on the shunt resistance.

The diode current (I_d) can be obtained using the classical diode current expression:

$$I_d = I_0 \left[\exp\left(\frac{qV_{oc}}{nKT_r}\right) - 1\right] \quad (2)$$

Where the diode current (I_d) in photovoltaic systems. Key parameters include I_0, the reverse saturation current; q, the elementary charge; V_{oc}, the open-circuit voltage; n, the ideality factor; K, the Boltzmann constant; and T_r, the diode temperature in Kelvin.

By substituting equation (2) into equation (1) and excluding the final term, the reformulated expression for the output current (I) is:

$$I = I_L - I_o \exp\left(\frac{q(V+IR_s)}{nKT_r} - 1\right) \quad (3)$$

In this context, the saturation current (I_o) at various operating temperatures can be computed according to the following expression [10]:

$$I_o = I_{o-T_r} * (\frac{T}{T_r})^{\frac{3}{n}} * \exp\left(\frac{-qV_g}{nK*(\frac{1}{T}-\frac{1}{T_r})}\right) \quad (4)$$

$$I_{o-T_r} = \frac{I_{sc-T_r}}{\exp\left(\frac{qV_{oc-T_r}}{nKT_r}\right)-1} \quad (5)$$

In equations (4) and (5), V_g denotes the band gap voltage, V_{oc-T_r} represents the open circuit voltage, and I_{sc-T_r} is the short circuit current under rated operating conditions.

The photocurrent I_L in equation (3) is directly correlated with the solar radiation level, G (W/m^2), and can be articulated as follows:

$$I_L = I_{L-T_r}(1 + \alpha_{I_{sc}}(T - T_r)) \quad (6)$$

Where,

$$I_{L-T_r} = \frac{G*I_{sc-T_r}}{G_r} \quad (7)$$

Here, $\alpha_{I_{sc}}$ represents the short circuit temperature coefficient.

The open circuit voltage V_{oc}, which is responsive to temperature changes, can also be derived as follows [9]:

$$V_{oc} = V_{oc-T_r}(1 - \beta_{V_{oc}}(T - T_r)) \quad (8)$$

In this context, $\beta_{V_{oc}}$ represents the open circuit temperature coefficient.

By utilizing coefficients provided by manufacturers and the mathematical expressions (3-8), any photovoltaic (PV) module can be characterized for dynamic analysis.

To elevate the produced DC voltage of the PV module to a desired level, a DC-DC boost converter can be employed, and the Maximum Power Point Tracking (MPPT) technique can be implemented in the boost converter to efficiently regulate the generated power from the PV arrays. Subsequently, the produced DC power is converted to AC power through a three-phase three-level Voltage Source Converter (VSC) and injected into the system via a coupling transformer.

2.2 PV characteristic

In the presented research framework, the Photovoltaic (PV) system exhibits notable characteristics, playing a pivotal role in the overall electrical distribution system. The PV modules utilized in the study are specified with a maximum power output of 305 watts, achieved at a voltage of 54.7 volts and a current of 5.58 amperes. The open-circuit voltage (Voc) is determined as 64.2 volts, and the short-circuit current (Isc) is recorded at 5.96 amperes. With an efficiency of 18.7%, these PV modules are configured into a system comprising 164 strings, each containing 10 modules, and resulting in a total of 1,640 modules within the array, with 96 cells per module.

Complementing the PV system, an inverter is employed to facilitate the integration of generated PV power into the grid. The inverter is characterized by a voltage rating of 230 volts, a power capacity of 500 kilowatts, and an efficiency of 95%. These parameters, combined with the detailed string and array configuration, encapsulate the essential electrical traits of both the PV system and the inverter, contributing valuable insights to the comprehensive analysis of the distributed power generation system under investigation as shown in Table 1and 2 [11].

TABLE 1. SOLAR PV MODULE SPECIFICATION

Sr. NO.	Characteristic	Value
1	Subfield Capacity	500 kW
2	Number of Strings	164
3	Modules per String	10
4	Cells per Module	96

TABLE 2. INFORMATION REGARDING THE PHOTOVOLTAIC MODULE AS OUTLINED IN THE DATASHEET.

Maximum Power (P_{max})	305 W
Voltage at Pmax (V_{mp})	54.7 V
Current at Pmax (I_{mp})	5.58 A
Open-circuit voltage (V_{oc})	64.2 V
Short-circuit current (I_{sc})	5.96 A
Efficiency	18.7%
Temperature coefficient of Current (I_{sc})	3.5 mA/°C
Temperature coefficient of Voltage (V_{oc})	–176.6 mV/°C
Temperature coefficient of power	–0.38% / °C

3. IEEE 9-Bus Network

The simulated power systems network, using the IEEE-9 Bus model as depicted in the single line diagram shown in Figure 3, will be examined in various operational scenarios outlined in subsequent sections. This network encompasses nine buses, 3 generators, 3 two-winding transformers, 6 lines, and 3 loads. The base voltage levels are 13.8 kV, 16.5 kV, 18.45 kV, and 230 kV. Each generator is portrayed as a voltage source with an arbitrarily set source impedance of 1 Ohm. Tables 3, 4, and 5 present the characteristic of IEEE-9 Bus system with a 100 MVA base.

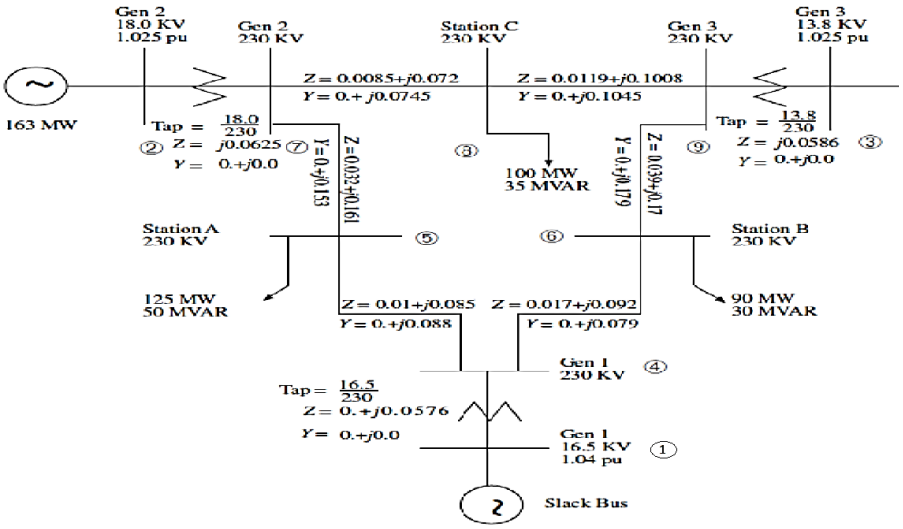

Figure 3. Diagram depicting the IEEE 9-Bus network in a single line.

TABLE 3. BUS DATA OF IEEE 9-BUS SYSTEM [12].

Bus	Bus Type	Voltage (P.U.)	Voltage (KV)	Generation		Load	
				MW	Mvar	MW	Mvar
1	Slack	1.04	16.5	0	0	0	0
2	PV	1.025	18.0	163	6.7	0	0
3	PV	1.025	13.8	85	-10.9	0	0
4	PQ	1	230	0	0	0	0
5	PQ	1	230	0	0	125	50
6	PQ	1	230	0	0	90	30
7	PQ	1	230	0	0	0	0
8	PQ	1	230	0	0	100	35
9	PQ	1	230	0	0	0	0

TABLE 4. LINE DATA OF IEEE 9-BUS SYSTEM [12].

Line From	Line To	R	X	B
1	4	0	0.0576	0
4	5	0.01	0.085	0.176
4	6	0.017	0.092	0.158
6	9	0.039	0.17	0.358
5	7	0.032	0.161	0.306
9	3	0	0.0586	0
7	2	0	0.0625	0
9	8	0.0119	0.1008	0.209
7	8	0.0085	0.072	0.149

TABLE 5. LOAD FLOW SOLUTION OF IEEE 9-BUS SYSTEM.

Bus	Generation		Load		Bus Vlotage	
	MW	Mvar	MW	Mvar	Voltage (p.u.)	Angle
1	71.6	27.0	0	0	1.04	0
2	163	6.7	0	0	1.025	9.3
3	85	-10.9	0	0	1.025	4.7
4	0	0	0	0	1.026	-2.2
5	0	0	125	50	0.996	-4.0
6	0	0	90	30	1.013	-3.7
7	0	0	0	0	1.026	3.7
8	0	0	100	35	1.016	0.7
9	0	0	0	0	1.032	2.0

3.1 Generator Bus:

This refers to the bus in the power system where a generator is connected. It's the point where electrical power is injected into the system [12].

3.2 Load Bus:

The load bus represents the point in the power system where electrical energy is consumed. It's the node where the load is connected, such as homes, industries, or other devices that draw power [12].

3.3 Devices Nodes:
These are various nodes in the power system where different devices or components may be connected. Devices can include transformers, capacitors, or other elements influencing the system's behavior.

3.4 Slack Node or Reference Bus:
The slack node, also known as the reference bus, is a bus in the power system that serves as a reference for the calculation of the load flow. Voltage magnitude and phase angle at this bus are typically specified, providing a reference for the rest of the network.

3.5 Bus Data:
This includes information about the buses in the system, such as voltage magnitudes, phase angles, and other relevant parameters. Bus data is crucial for load flow computation as it forms the basis for analyzing the electrical state of each node.

3.6 Line Data:
Line data involves information about the transmission lines connecting different buses. This includes parameters like line impedance, admittance, and other characteristics influencing the flow of electrical power between nodes.

In summary, Load Flow Computation in the IEEE 9-bus system entails analyzing the power distribution among generator buses, load buses, and devices nodes. The slack node provides a reference, and data about buses and lines is used to calculate voltage magnitudes, angles, and power flows, ensuring the system operates within acceptable limits [13].

4. HARMONIC DISTORTION

Harmonic distortion poses a significant issue in electrical power systems, impacting power quality. It involves the alteration of the normal voltage or current waveform, deviating from its original shape or characteristics. Typically, sources of harmonic distortion include rectifiers, nonlinear loads, power converters, transformers, and rotating machines [14]. Given that PV systems incorporate various power-electronic devices that generate distortion, inverters, which play a crucial role in Grid-Connected Photovoltaic Power Plants (GCPPP), are no exception. Within the context of PV inverters connected to the grid, two key factors are efficiency and the quality of electricity supply.

To assess electricity supply quality, an examination of THD in current and voltage is essential. THD serves as a metric to quantify the presence of harmonics in a power system. For a voltage or current waveform, THD is defined as the ratio of the sum of all magnitudes of voltage or current harmonic components to the magnitude of the fundamental frequency. The expression for calculating THD is as follows [15,20]:

To calculate the THD using the Fast Fourier Transform (FFT) for an IEEE 9-bus system connected with a photovoltaic (PV) system, you'll need to follow several steps. Below, I'll outline the general procedure and equations involved:

1. Data Collection: Gather the necessary data for the IEEE 9-bus system and the PV system, including voltage and current measurements.

2. FFT Calculation: Apply the FFT algorithm to the voltage and current waveforms to transform them from the time domain to the frequency domain. This will provide you with the magnitude and phase of each harmonic component.

3. Harmonic Amplitude Calculation: Determine the amplitude of each harmonic component from the FFT results. This involves summing the magnitudes of the individual harmonics.

4. Fundamental Component Calculation: Calculate the magnitude of the fundamental frequency component. This is typically the first harmonic, representing the fundamental frequency (e.g., 50 Hz or 60 Hz).

5. THD Calculation: Use the formula for THD to determine the percentage of harmonic distortion relative to the fundamental frequency component. The THD formula is:

$$THD = \frac{\sqrt{\sum_{n=2}^{N}(V_n)^2}}{V_i} * 100 \quad (9)$$

Where:

V_n is the amplitude of the nth harmonic component.

V_i is the amplitude of the fundamental frequency component.

N is the highest harmonic order considered in the calculation (typically limited to a certain order to avoid numerical errors and to focus on significant harmonics).

6. Analysis and Interpretation: Analyze the THD results to assess the level of harmonic distortion in the system. Compare the calculated THD values with the relevant standards or guidelines to evaluate compliance.

Below is a more detailed breakdown of the steps with equations:

4.1 FFT Calculation

Apply the FFT algorithm to voltage and current waveforms to obtain their frequency domain representations:

$$X(f) = FFT\ ((x(t)) \quad (10)$$

Where:

$X(f)$ is the frequency domain representation of the signal.

$x(t)$is the time-domain signal.

4.2 Harmonic Amplitude Calculation

For each harmonic component, calculate its magnitude:

$$V_n = \sqrt{(R_e(X(f_n)))^2 + (I_m(X(f_n)))^2} \quad (11)$$

Where:

V_n is the amplitude of the nth harmonic component.

$R_e(X(f_n))$ is the real part of the FFT result at frequency f_n.

- $I_m(X(f_n))$ is the imaginary part of the FFT result at frequency f_n.

4.3 Fundamental Component Calculation

Determine the magnitude of the fundamental frequency component:

$$V_1 = \sqrt{(R_e(X(f_1)))^2 + (I_m(X(f_1)))^2} \quad (12)$$

Where:

V_1 is the amplitude of the fundamental frequency component.

f_1 is the frequency of the fundamental component.

4.4 THD Calculation

Use the formula for THD to calculate the percentage of harmonic distortion:

$$THD = \frac{\sqrt{\sum_{n=2}^{N}(V_n)^2}}{V_1} * 100 \quad (13)$$

Where:

V_n is the amplitude of the nth harmonic component.

V_1 is the amplitude of the fundamental frequency component.

N is the highest harmonic order considered in the calculation.

Figure. 4 illustrates the proposed methodology's flowchart.

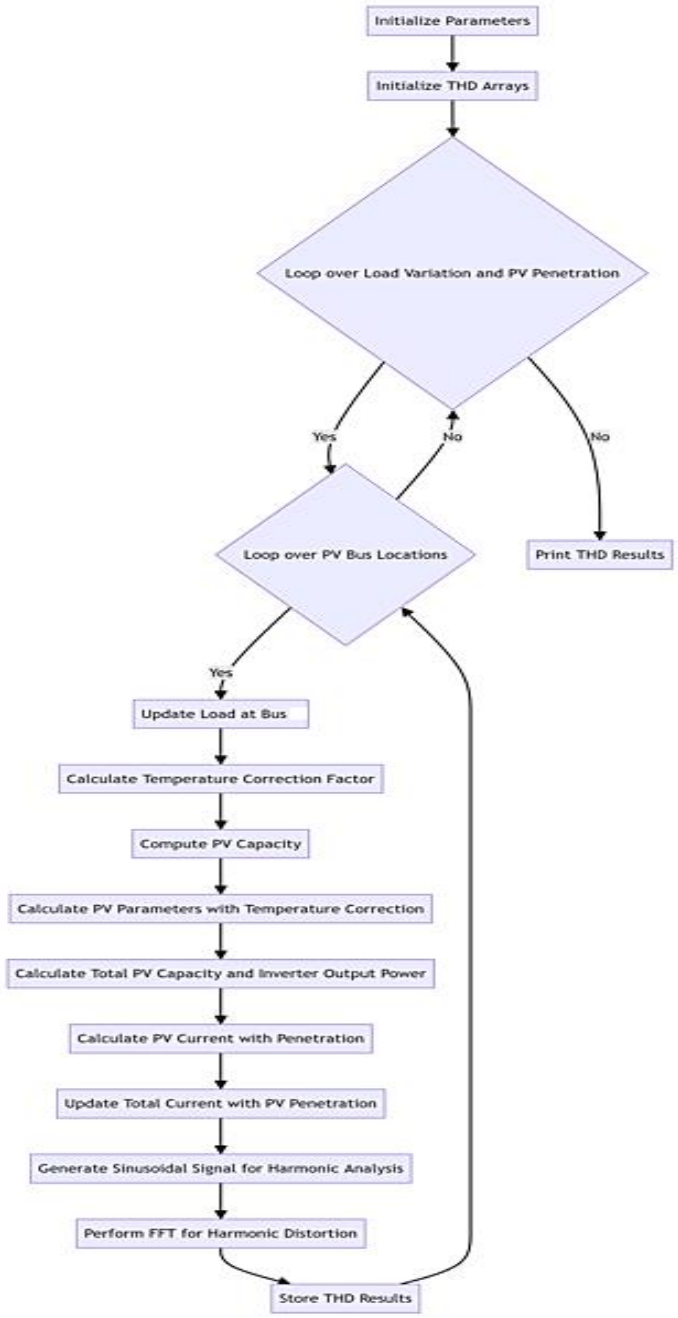

Figure 4. The flowchart outlining the proposed methodology to cal

5. CASE STUDY

5.1 case 1

In this scenario, the load on bus 8 gradually increases from 5% (5 MW) to 25% (25 MW) of its standard capacity (100 MW), incrementing in steps of 5% (5 MW). To offset this rise, a PV system is introduced. The main objective is to determine the best location for the PV system to minimize the maximum THD across the entire system. Consequently, THD analysis is performed sequentially as the PV system is connected to bus 5, bus 6, and bus 8. Additionally, the PV penetration varies from 5% to 25% in steps of 5% for each case of load variation.

TABLE 6. THE MAXIMUM THD RESULTING FROM LOAD VARIATION AND PV PENETRATION OCCURS AT BUS 8.

Load Variation	PV Penetration	THD Bus 5	THD Bus 6	THD Bus 8
5%	5%	10.4024%	7.4872%	8.7366%
	10%	10.3934%	7.4781%	8.7275%
	15%	10.3843%	7.4691%	8.7185%
	20%	10.3752%	7.4600%	8.7094%
	25%	10.3662%	7.4510%	8.7004%
10%	5%	10.4024%	7.4872%	9.1530%
	10%	10.3934%	7.4781%	9.1440%
	15%	10.3843%	7.4691%	9.1349%
	20%	10.3752%	7.4600%	9.1259%
	25%	10.3662%	7.4510%	9.1168%
15%	5%	10.4024%	7.4872%	9.5695%
	10%	10.3934%	7.4781%	9.5604%
	15%	10.3843%	7.4691%	9.5514%
	20%	10.3752%	7.4600%	9.5423%
	25%	10.3662%	7.4510%	9.5333%
20%	5%	10.4024%	7.4872%	9.9860%
	10%	10.3934%	7.4781%	9.9769%
	15%	10.3843%	7.4691%	9.9678%
	20%	10.3752%	7.4600%	9.9588%
	25%	10.3662%	7.4510%	9.9497%
25%	5%	10.4024%	7.4872%	10.4024%
	10%	10.3934%	7.4781%	10.3934%
	15%	10.3843%	7.4691%	10.3843%
	20%	10.3752%	7.4600%	10.3752%
	25%	10.3662%	7.4510%	10.3662%

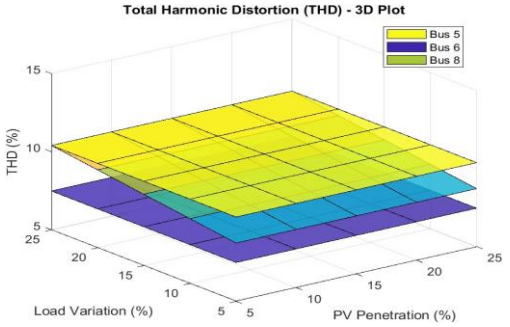

Figure 5. The maximum THD resulting from load variation and PV penetration occurs at bus 8.

The results reveal a clear relationship between the maximum THD and the size of the PV system, as depicted in Figure. 5 and Tables 6. Additionally, the lowest THD is achieved by connecting the PV system to bus 6, considering fluctuations in both load conditions and PV penetration.

5.2 case 2

In this specific scenario, the load at bus 5 varies from 5% to 25% of its rated capacity (125 MW), with a step size of 5%. To counteract these load fluctuations, a PV system is introduced, with its rating adjusted to match the load changes in each step. The primary goal is to determine the optimal location for the PV system (bus 6, 5, or 8) in order to minimize the maximum THD within the system. As a result, the PV system is assumed to be sequentially connected to bus 5, 6, and 8. Additionally,

PV penetration varies from 5% to 25% in each case of load variation.

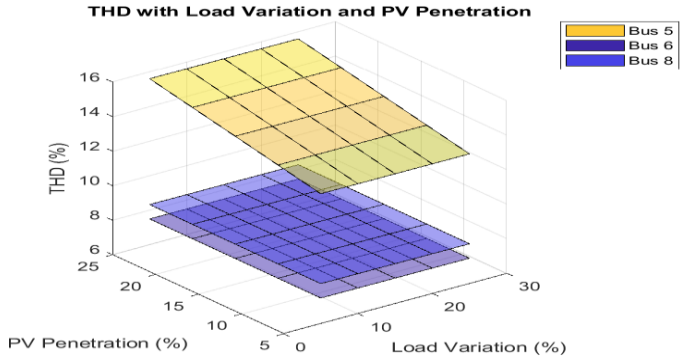

Figure 6. The maximum THD resulting from load variation and PV penetration occurs at bus 5.

Table 7. The maximum THD resulting from load variation and PV penetration occurs at bus 5.

Load Variation	PV Penetration	THD Bus 5	THD Bus 6	THD Bus 8
5%	5%	13.5258%	7.4872%	8.3201%
	10%	13.5168%	7.4781%	8.3111%
	15%	13.5077%	7.4691%	8.3020%
	20%	13.4987%	7.4600%	8.2930%
	25%	13.4896%	7.4510%	8.2839%
10%	5%	14.0464%	7.4872%	8.3201%
	10%	14.0374%	7.4781%	8.3111%
	15%	14.0283%	7.4691%	8.3020%
	20%	14.0193%	7.4600%	8.2930%
	25%	14.0102%	7.4510%	8.2839%
15%	5%	14.5670%	7.4872%	8.3201%
	10%	14.5579%	7.4781%	8.3111%
	15%	14.5489%	7.4691%	8.3020%
	20%	14.5398%	7.4600%	8.2930%
	25%	14.5308%	7.4510%	8.2839%
20%	5%	15.0876%	7.4872%	8.3201%
	10%	15.0785%	7.4781%	8.3111%
	15%	15.0695%	7.4691%	8.3020%
	20%	15.0604%	7.4600%	8.2930%
	25%	15.0514%	7.4510%	8.2839%
25%	5%	15.6081%	7.4872%	8.3201%
	10%	15.5991%	7.4781%	8.3111%
	15%	15.5900%	7.4691%	8.3020%
	20%	15.5810%	7.4600%	8.2930%
	25%	15.5719%	7.4510%	8.2839%

As depicted in Figure. 6 and Tables 7 the THD demonstrates a direct correlation with the magnitude of the PV system. Furthermore, connecting the PV system to bus 6 under various loading conditions achieves the lowest THD throughout the system.

5.3 case 3

In this particular scenario, the load at bus 6 fluctuates from 5% (4.5 MW) to 25% (22.5 MW) of its rated capacity (90 MW) in increments of 5% (4.5 MW). A PV system is introduced to offset these variations, with the PV system rating matching the load change in each step. The primary objective is to identify the optimal location for the PV system (bus 6, 5, or 8) to minimize

the maximum THD within the system. Consequently, the PV system is assumed to be connected sequentially to bus 5, 6, and 8. Additionally, PV penetration varies from 5% to 25% in each case of load variation.

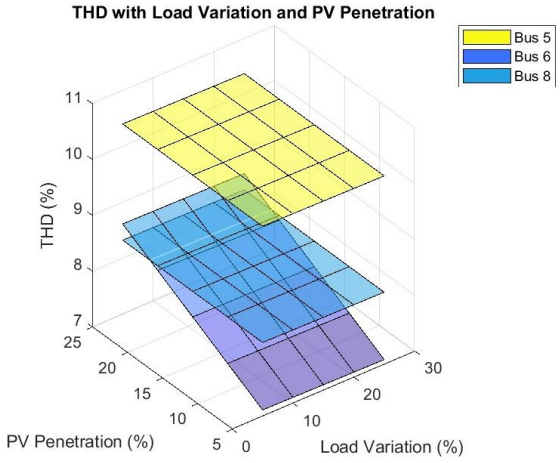

Figure 7. The maximum THD resulting from load variation and PV penetration occurs at bus 6.

TABLE 8. THE MAXIMUM THD RESULTING FROM LOAD VARIATION AND PV PENETRATION OCCURS AT BUS 6.

Load Variation	PV Penetration	THD Bus 5	THD Bus 6	THD Bus 8
5%	5%	10.4024%	7.1124%	8.3201%
	10%	10.3934%	7.1033%	8.3111%
	15%	10.3843%	7.0943%	8.3020%
	20%	10.3752%	7.0852%	8.2930%
	25%	10.3662%	7.0762%	8.2839%
10%	5%	10.4024%	7.4872%	8.3201%
	10%	10.3934%	7.4781%	8.3111%
	15%	10.3843%	7.4691%	8.3020%
	20%	10.3752%	7.4600%	8.2930%
	25%	10.3662%	7.4510%	8.2839%
15%	5%	10.4024%	7.8620%	8.3201%
	10%	10.3934%	7.8530%	8.3111%
	15%	10.3843%	7.8439%	8.3020%
	20%	10.3752%	7.8349%	8.2930%
	25%	10.3662%	7.8258%	8.2839%
20%	5%	10.4024%	8.2368%	8.3201%
	10%	10.3934%	8.2278%	8.3111%
	15%	10.3843%	8.2187%	8.3020%
	20%	10.3752%	8.2097%	8.2930%
	25%	10.3662%	8.2006%	8.2839%
25%	5%	10.4024%	8.6116%	8.3201%
	10%	10.3934%	8.6026%	8.3111%
	15%	10.3843%	8.5935%	8.3020%
	20%	10.3752%	8.5845%	8.2930%
	25%	10.3662%	8.5754%	8.2839%

As depicted in Figure 7 and detailed in Tables 8, a noticeable positive correlation exists between the THD and the magnitude of the PV system. Notably, connecting the PV system to bus 6 under various load conditions consistently yields the lowest

THD across the entire system, with the exception occurring at the 25% load variation. Nevertheless, across the range of load changes from 5% to 25%, bus 6 consistently achieves the minimum THD compared to other locations.

6. CONCLUSION

In this research paper, we have explored the dynamics of power distribution in the IEEE 9-bus system under various operational scenarios and analyzed the impact of introducing PV systems on THD within the network. Through a systematic investigation involving three distinct case studies, we have elucidated valuable insights into optimizing the placement of PV systems to minimize THD and enhance power quality.

Our analysis revealed a significant correlation between the size of the PV system and the maximum THD across the system. By sequentially connecting the PV system to different buses (5, 6, and 8) under varying load conditions and penetration levels, we demonstrated the effectiveness of strategically placing PV systems to mitigate THD. Particularly, connecting the PV system to bus 6 consistently resulted in the lowest THD levels across the system, offering a promising strategy for enhancing power quality.

Furthermore, this study emphasized the importance of considering both load variations and PV penetration levels when assessing the impact on THD. By systematically varying these parameters, we provided comprehensive insights into the behavior of the system under different operating conditions, enabling informed decision-making in real-world applications.

Additionally, this paper proposed a methodology for calculating THD using FFT analysis, offering a practical approach for evaluating harmonic distortion in complex power systems such as the IEEE 9-bus network. This methodology can serve as a valuable tool for power engineers and researchers in assessing and optimizing power quality in grid-connected photovoltaic systems.

In conclusion, this research contributes to the advancement of understanding and optimizing power distribution systems with renewable energy integration. By elucidating the relationship between PV system placement and THD reduction, we pave the way for more efficient and sustainable power infrastructure, ultimately benefiting both utilities and end-users in terms of reliability and quality of electricity supply.

REFERENCES

[1] Hota, Akansha, et al. “Modeling & Simulation of Photovoltaic System Connected to Grid Using Matlab.” 2020 International Conference on Renewable Energy Integration into Smart Grids: A Multidisciplinary Approach to Technology Modelling and Simulation (ICREISG), IEEE, 2020.

[2] Abdelhady Ramadan, Salah Kamel, and Abdalla A. Ibrahim, “Parameters Estimation of Photovoltaic Cells Using Self-Adaptive Multi-Population Rao Optimization Algorithm.” 2021. Aswan University Journal of Sciences and Technology 1 (1): 26–40. https://doi.org/10.21608/aujst.2021.226476.

[3] Alshammari, M., & Hurley, W. G. (2022). A comparative study between four maximum power point tracking techniques for photovoltaic array system under partial shading conditions. https://doi.org/10.36227/techrxiv.20682382.v1

[4] M. H. El-Ahmer, Abou-Hashema M. El-Sayed, and A. M. Hemeida, "Mathematical modeling of Photovoltaic module and evalute the effect of varoius paramenters on its performance", 2016 Eighteenth International Middle East Power Systems Conference (MEPCON), Cairo, Egypt, 27-29 December 2016.

[5] Kazmierkowski, Marian P. “Power Electronics for Renewable Energy Systems, Transportation and Industrial Applications [Book News].” IEEE Industrial Electronics Magazine, vol. 8, no. 4, 2014, pp. 68–69, https://doi:10.1109/mie.2014.2361240.

[6] Khalid Hailan, Saif Aldeen, and Riyadh G. Omar. “Harmonics Compensation for Grid Connected to PV System Using Two-Step Finite Set Predictive Control.” 2022 Iraqi International Conference on Communication and Information Technologies (IICCIT), IEEE, 2022.

[7] Balram, Gyadari, and P. Satish Kumar. “Harmonics Reduction and Balanced Transition in Hybrid Renewable Energy Sources in a Micro Grid Power System.” Journal of New Materials for Electrochemical Systems, vol. 26, no. 4, 2023, pp. 233–242, https://doi:10.14447/jnmes.v26i4.a01.

[8] Charalambous, Charalambos A., et al. “Effects of Electromagnetic Interference on Underground Pipelines Caused by the Operation of High Voltage AC Traction Systems: The Impact of Harmonics.” IEEE Transactions on Power Delivery, vol. 33, no. 6, 2018, pp. 2664–2672, doi:10.1109/tpwrd.2018.2803080.
[9] P. Jayakumar and P. Reji, “Modeling of power distribution feeder and analysis of small PV plant penetration in Kerala low voltage distribution system,” in 2016 International Conference on Cogeneration, Small Power Plants and District Energy (ICUE), 2016. https://doi.org/10.1109/COGEN.2016.7728944
[10] S. R. Wenham, M. A. Green, M. E. Watt, and R. Corkish, "Applied Photovoltaics," Routledge, 2013. https://doi.org/10.3390/su132011435.
[11] Www.Sunpowercorp, http://www.sunpowercorp,. Accessed 9 Apr. 2024.
[12] K.Loji,I.E.Davidson,andR.Tiako,"VoltageprofileandpowerlossesanalysisonamodifiedIEEE9−bussystemwithPVpenetrationatthedistributionendsin2019 Southern African Universities Power Engineering Conference/Robotics and Mechatronics/Pattern Recognition Association of South Africa (SAUPEC/RobMech/PRASA),2019.https://doi.org/10.1109/robomech.2019.8704802
[13] P. M. Anderson and A. A. Fouad, "Power System Stability and Control Series," McGraw-Hill Inc., ISBN 0-07-035958-X, California, 1994.
[14] Seme, S., Lukač, N., Štumberger, B., & Hadžiselimović, M. (2017). Power quality experimental analysis of grid-connected photovoltaic systems in urban distribution networks. Energy (Oxford, England), 139, 1261–1266. https://doi.org/10.1016/j.energy.2017.05.088
[15] Ayub, M., Gan, C. K., & Kadir, A. F. A. (2014). The impact of grid-connected PV systems on Harmonic Distortion. 2014 IEEE Innovative Smart Grid Technologies - Asia (ISGT ASIA).
[16] F. Shahnia, A. Ghosh, G. Ledwich, and F. Zare, "Voltage correction in low voltage distribution networks with rooftop PVs using custom power devices," in IECON 2011-37th Annual Conference on IEEE Industrial Electronics Society, 2011, pp. 991-996
[17] Doaa Muhamed Hasanin, Ayat Ali Saleh, Mountasser M. M. Mahmoud, “Multi-Objective Self-Adaptive a Non-Dominated Sorting Genetic (NSGA) Algorithm for Optimal Sizing of PV/Wind/Diesel Hybrid Microgrid System.” Aswan University Journal of Sciences and Technology, vol. 1, no. 2, 2021, pp. 1–15, https://doi:10.21608/aujst.2021.226485.
[18] A. Q. Al-Shetwi and M. Sujod, "Design and Economic Evaluation of Electrification of Small Villages in Rural Area in Yemen Using Stand-Alone PV System," *International Journal of Renewable Energy Research (IJRER)*, vol. 6, pp. 1442-1451, 2016.
[19] H. Wu and X. Tao, "Three phase photovoltaic grid-connected generation technology with MPPT function and voltage control," in *2009 International Conference on Power Electronics and Drive Systems (PEDS)*, 2009, pp. 1295-1300.
[20] V. R. F. B. de Souza, M. Alves Filho, and K. C. de Oliveira, "Analysis of power quality for photovoltaic systems connected to the grid," in *Harmonics and Quality of Power (ICHQP), 2016 17th International Conference on*, 2016, pp. 226-230.